Magnetic Retrieval of Encapsulated Beta Cell Transplants from Diabetic Mice Using Dual# Function MRI Visible and Retrievable Microcapsules

Magnetic retrieval of encapsulated beta cell transplants from diabetic mice using dual-function MRI visible and retrievable microcapsules

*Derfogail Delcassian[1,2,3,4], Igor Luzhansky[1,2], Virginia Spanoudaki[1,2], Matthew Bochenek[1,2,3], Collin McGladrigan[1,2], Amy Nyugen[1,2], Samuel Norcross[1,2], Yuhan Zhu[1,2], Crystal Shuo Shan[1,2], Reed Hausser[1,2], Kevin M. Shakesheff[4], Robert Langer[1,2,3,5,6,7], Daniel G. Anderson [1,2,3,5,6,7]**

1. David H Koch Institute for Integrative Cancer Research, Massachusetts Institute of Technology, 500 Main Street, Cambridge, MA 02139, USA

2. Department of Anesthesiology, Boston Children's Hospital, 300 Longwood Ave, Boston, MA 02115, USA

3. Department of Chemical Engineering, Massachusetts Institute of Technology, 77 Massachusetts Avenue, Cambridge, MA 02139, USA

4. Division of Regenerative Medicine and Cellular Therapies, University of Nottingham, Nottingham, NG7 2RD, UK

5. Howard Hughes Medical Institute, Harvard University, Cambridge, MA 02138, USA

6. Division of Health Science Technology, Massachusetts Institute of Technology, 77 Massachusetts Avenue, Cambridge, MA 02139, USA

7. Institute for Medical Engineering and Science, Massachusetts Institute of Technology, 77 Massachusetts Avenue, Cambridge, MA 02139, USA

***Corresponding author**; Daniel G. Anderson, dgander@mit.edu

Keywords: magnetic retrieval, nanoparticle, encapsulated cell therapy, islet transplantation, MRI

Abstract

Encapsulated beta cell transplantation offers a potential cure for a subset of diabetic patients. Once transplanted, beta cell grafts can help to restore glycemic control, however, locating and retrieving cells in the event of graft failure may pose a surgical challenge. Here, we have developed a dual-function nanoparticle-loaded hydrogel microcapsule which enables graft retrieval under an applied magnetic field. Additionally, this system facilitates graft localization *via* magnetic resonance imaging, and graft isolation from the immune system. We transplanted iron oxide nanoparticles encapsulated within alginate hydrogel capsules containing viable islets. We compared the *in vitro* and *in vivo* retrieval of capsules containing nanoparticles functionalized with various ligands. Capsules containing islets co-encapsulated with COOH-coated nanoparticles restore normal glycaemia in immunocompetent, diabetic mice for at least 6 weeks, can be visualized using MRI, and are retrievable in a magnetic field. Application of a magnetic field for 90 seconds *via* a magnetically assisted retrieval device facilitated rapid retrieval of up to 94% (+/- 3.1%) of the transplant volume 24 hours after surgical implantation. This strategy aids monitoring of cell-capsule locations *in vivo*, facilitates graft removal at the end of the transplant lifetime, and may be applicable to many encapsulated cell transplant systems.

Introduction

For patients with diabetes, islet transplantation can help to restore insulin secretion and long-term normoglycemia,[1, 2] offering a potential alternative to daily insulin injections. In this procedure islets are isolated from a donor pancreas and are typically transplanted into the liver *via* hepatic portal vein infusion.[3, 4] This often requires patients to take systemic immunosuppressants to prevent graft rejection. Additionally, retrieval of these grafts from the liver in the event of graft failure remains surgically challenging and risks injury to the host.[5]

In an alternative approach, cell and organoid grafts can be encapsulated within hydrogel materials prior to transplantation.[6-9] The hydrogels help to physically isolate the graft from the host immune system, reducing the need for systemic immunosuppression, and limit cellular rejection following transplantation.[10, 11] Recently, chemically modified hydrogels have been developed which can also reduce foreign body responses and associated material fibrosis.[8, 12] This has enabled the transplant of cell and organoid therapies to a wider range of accessible extra-hepatic transplant sites in small animal models and non-human primates.[8, 9]

As these cell and organoid transplantation systems are translated to humans, it is increasingly important to develop strategies to monitor the location of transplanted and encapsulated cell systems. There may also be a need for methods that facilitate removal of transplanted grafts in the event of graft failure post-transplantation. This is of particular interest for capsule based micro-encapsulation systems, where a curative transplant would require many capsules containing encapsulated islets. [13, 14] To address this challenge, we sought to develop methods that enable both monitoring and retrieval of encapsulated cell and organoid therapies.

Transplanted islets have previously been tracked *in vivo* through cellular labelling with fluorescent dyes, nanoparticle based contrast agents, or radiolabels. [15-23] Co-encapsulation

of contrast agents within hydrogels capsules has also been used to locate encapsulated islets *via* magnetic resonance imaging (MRI) *in vitro* [21, 24] and recently, to track the movement of unconstrained capsules implanted *in vivo*[25]. Although these strategies facilitate localization of implanted capsules, they do not directly facilitate the retrieval of such implanted grafts. We have developed a dual-function hydrogel capsule, which can facilitate graft retrieval under a directed magnetic field and aids graft localization *via* magnetic resonance imaging (MRI).

Here, we show the first example of an encapsulated cell therapy which can be magnetically retrieved following transplantation. Our system provides a single integrated approach for both *in vivo* capsule localisation and retrieval. We demonstrate the therapeutic use of these materials to transplant encapsulated rat islets into immunocompetent diabetic mice. These technologies provide a tool for the encapsulation of a range of functional cells and cell organoids with dual imaging/retrieval capabilities and facilitate graft monitoring and graft removal at the end of the transplant lifetime.

Results and Discussion

Design of nanoparticle loaded hydrogels

Alginate hydrogels can be used for cell encapsulation and transplant. Hydrogel capsules can be formed through electrostatic droplet generation, followed by divalent cation crosslinking of guluronic acid residues on the alginate polymer backbone, shown schematically in **Figure 1A.**[26] To develop hydrogel capsules which can be magnetically retrieved, we incorporated iron oxide nanoparticles coated with different functional groups into the hydrogel aqueous phase before droplet generation (detailed in materials and methods). We hypothesized that interactions between functional groups on the surface of the nanoparticles, carboxylic acid groups in the guluronate block within alginate, and divalent cations used during alginate crosslinking may stabilize nanoparticle-hydrogel interactions.[27] This could enable

production of hydrogel capsules which respond to magnetic fields and are suitable for co-encapsulation with viable cells for long-term implantation and retrieval *in vivo.*

Three iron oxide nanoparticle systems were tested; unfunctionalized nanoparticles (NP), nanoparticles functionalized with poly-ethylene glycol (NP-PEG), or nanoparticles functionalized with carboxylic acid groups (NP-COOH). Functionalized nanoparticles were well dispersed, spherical, and roughly 30nm in diameter (Figure 1B, NP-COOH: diameter 29.6nm +- 1.4nm SD , NP-PEG: diameter 28.8nm +- 2.3nm SD) whilst unfunctionalized nanoparticles (NP) had a wider distribution of aggregated spherical, ovoid and cuboid shapes apparent by TEM (diameter 15.4nm +- 7.2nm SD). We next tested the electrostatic properties of these systems. Zeta potential measurements for NP, NP-COOH and NP-PEG nanoparticles were -37.5mV (0.7mV SD), -37.3 (1.7mV SD) and -18.5 (1.4mV SD) respectively (Figure 1D,E).

Magnetic mobility of nanoparticle loaded hydrogels

Hydrogel capsules with iron oxide concentrations between 0-5mg/ml were made at two clinically relevant capsule sizes (0.5mm and 1.5mm)[9, 14] and the mobility of these capsules in a magnetic field was tested. To explore capsule response to magnetic fields, we measured the distance at which capsules containing nanoparticles were able to move through saline (against gravity) towards a magnet at a fixed distance (Figure 1E-H, Supporting Information Video 1). Briefly, capsules were placed in the bottom of a syringe filled with saline, allowed to settle, and then a magnetic plunger was slowly lowered in the syringe. The distance from the magnet at which 1x 1.5mm capsule, or 2x 0.5mm capsules moved towards the magnet was recorded. All three nanoparticle loaded systems were magnetically responsive. As expected, the distance which capsules could cross towards a magnet increased as nanoparticle concentration increased, demonstrating that the retrieval distance is proportional to nanoparticle concentration at loadings between 0.1-5mg/ml, with

responsiveness ranked as NP-COOH > NP-PEG > unfunctionalized-NP nanoparticles. In all cases, at loading densities above 1mg/ml, capsules could be collected on magnets positioned 1-2 cm away *in vitro*, which suggested a dynamic retrieval range suitable for magnetically assisted retrieval of capsules surgically implanted in mice. At this concentration, the NP-COOH capsules are significantly more responsive (can be retrieved at greater distances) than the NP or NP-PEG systems. There was no statistical difference in retrieval distance between large and small capsules (Figure1H, Supporting Information (SI) Figure 1).

We investigated the stability and mechanical properties of hydrogels containing various nanoparticles to determine suitability for cell encapsulation and potential transplantation. We compared the hydrogel morphology (Figure 1B), electrostatic interactions (Figure 1C,D), mechanical properties (SI Figure 2) and long-term nanoparticle retention (SI Figure 3). In general, nanoparticle loaded alginate capsules can be formed up to a nanoparticle loading density of 1-2.5mg/ml. Above this threshold, there is some disruption to the spherical morphology of the capsules, inducing "tail" formation (Figure 1B, indicated by the white circles), particularly in NP-PEG systems (SI Figure 5-7). We evaluated storage (G') and loss modulus (G") of different gels in response to strain using a rheometer across the frequency range 0.2 rad/s to 150 rad/s. This allows us to evaluate if inclusion of nanoparticles significantly alters the mechanical properties of the hydrogels. In all systems, viscoelastic hydrogels were formed, with G' an order of magnitude greater than G" (SI Figure 2).

We used a spectroscopic approach to assess nanoparticle leaching and the long-term stability of these nanoparticle loaded hydrogel systems. Iron oxide nanoparticles strongly absorb in the 300-400nm wavelength range; we assessed UV-Vis absorbance of supernatants taken from gels incubated in calcium supplemented saline for up to 6 months (SI Figure 3). NP and NP-COOH capsules were stable, with no detectable nanoparticle leaching over a 6 month timeframe. In contrast, leaching of NP-PEG nanoparticles from the NP-PEG hydrogel capsules occurred over a 6 month timeframe (<0.2mg/ml, SI Figure 3). This data suggests that

the NP-PEG alginate hydrogel system is not stable, and that NP-PEG nanoparticles are able to move within and out of the hydrogel matrix over time.

As capsule formation occurs *via* an electrostatic droplet generation system, it is possible that changes in the electrostatic interactions of the alginate/nanoparticle mixture may affect capsule integrity. Zeta potential of nanoparticles in alginate solutions (Figure 1D) and conductivity studies (Figure 1C) indicated that NP and NP-PEG nanoparticles in alginate significantly altered the electrostatic properties of alginate solutions, in contrast to NP-COOH systems which did not alter alginate conductivity. COOH functionalized nanoparticles may also interact electrostatically *via* complexation between the divalent cation and COOH groups on the nanoparticle and alginate backbone to form a more stable hydrogel system better suited for cell encapsulation (Figure 1A schematic).

Figure 1: Properties of iron oxide nanoparticle and nanoparticle loaded hydrogels (A1,2) Schematic of nanoparticle loaded hydrogel capsules (A1) formation and (A2) application in diabetes transplants with MRI imaging and magnetic retrieval capabilities. (B) TEM images of the different nanoparticle systems used and microscopy images of alginate hydrogel capsules containing nanoparticles at loading densities from 0.25mg/ml to 5mg/ml. (C) Conductivity and (D) zeta potential of nanoparticles in saline or a saline-alginate aqueous phase. Statistical analysis performed using one way ANOVA with multiple comparisons, statistics represent comparison to nanoparticles suspended in alginate. (E-H) Magnetic retrieval of nanoparticle loaded hydrogels in saline against gravity (E) Video stills of the magnetic retrieval process (stills time = zero, time= 16 seconds, and time= 22 seconds) (F) comparison between retrieval distances (the distance at which the first capsule moves against gravity towards the magnet) for NP, NP-COOH and NP-PEG 1.5mm alginate hydrogel capsules at concentrations between 0.25mg/ml and 5mg/ml (G,H) average retrieval distance for 1.5mm capsules at 1mg/ml iron oxide loading, and a comparison between capsules of different sizes. Statistical analysis performed using one way ANOVA with multiple comparisons, statistics represent comparison to nanoparticles suspended in alginate. All graphs show mean values +/- SEM with $p<0.05$*, $p<0.01$**, $p<0.001$***, $p<0.0001$****.

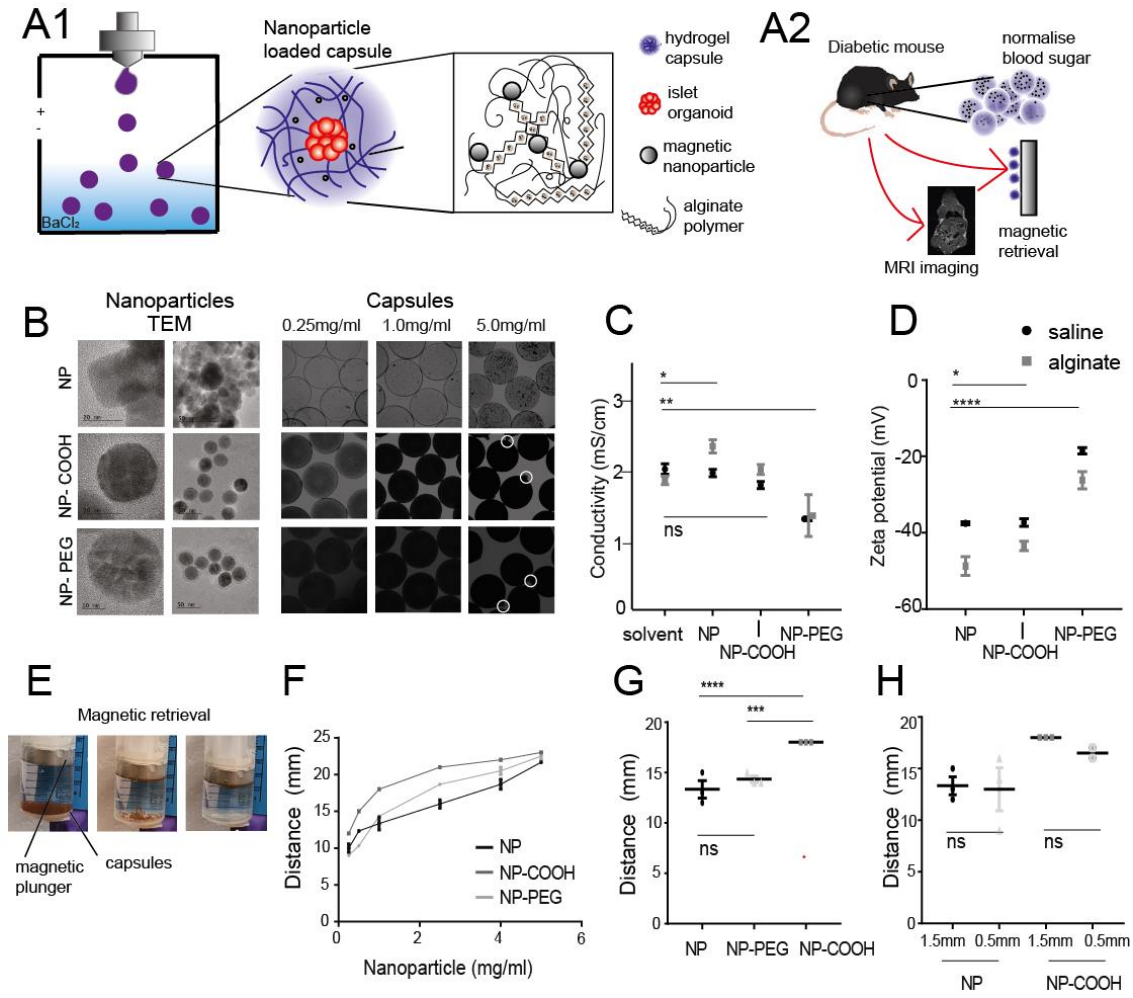

Cellular behavior in nanoparticle loaded hydrogels

We evaluated the effect of various iron oxide nanoparticles on primary rat islets *in vitro*. Islets were co-cultured with various nanoparticle systems (no nanoparticle or unfunctionalized NPs, NP-COOH, or NP-PEG nanoparticles) for 48 hours. Islet viability was then evaluated using Calcein AM staining and metabolic activity using a luciferase ATP assay. We found that the percentage of viable cells per islet remains consistent across these conditions (Figure 2B; median 94.0% in untreated cells, and 92.0, 94.5 and 95.5% for NP, NP-COOH and NP-PEG respectively) compared to islets treated with ethanol for 1.5 hours (28.0% viable). We also compared the metabolic activity of islets following treatment with nanoparticles, using a luciferase assay to quantify ATP activity within cells. Figure 2C illustrates that there is a slight (non-significant) decrease in mean ATP activity within islets (19.5, 25.1, 24.0% decrease in ATP activity for NP, NP-COOH and NP-PEG respectively) following incubation with nanoparticles.

Next, islets were encapsulated in alginate systems containing the three different iron oxide nanoparticles at 1mg/mL, and the secretion of insulin in response to glucose stimulation was monitored. Encapsulated islets were exposed to basal low (2mM) and high glucose (20mM) solutions and the stimulation index was calculated at 24 hours post-encapsulation. In the absence of nanoparticles, islets demonstrated a 5.5-fold increase in insulin secretion following exposure to low and high glucose conditions post encapsulation. Islets co-encapsulated with NP (unfunctionalized) and NP-COOH (COOH functionalized) nanoparticles showed a similar trend (5.1 and 5.2 fold increase respectively). Islets co-encapsulated with NP-PEG (PEG functionalized) nanoparticles showed a decreased stimulation index at 24 hours (stimulation index 2.6), suggesting impaired cellular function. Earlier, we found that NP-PEG functionalized nanoparticles leached from capsules (SI Figure 2). PEG ligands are often included in nanoparticle delivery systems due to their ability to improve nanoparticle circulation times and facilitate penetration of specific biological

barriers.[28-32] It is possible that the disruption to beta cell function may be related to NP-PEG leaching or cellular penetration however further studies on the interaction between islets and nanoparticles would be required to understand the precise biological mechanism driving this effect. In all cases, islets encapsulated with nanoparticles demonstrated suppressed insulin secretion and ATP activity compared to islets alone, although this was not significant.

Figure 2: Islet function in encapsulated nanoparticle systems (A) Schematic; islets were cultured for 48 hours with 1- media,2- 0.1mg/ml unfunctionalised nanoparticles, 3- 0.1mg/ml NP-COOH, 4- 0.1mg/ml NP-PEG for 48 hours or 5- 70% ethanol for 1.5hours. (A1-A5) Microscopy of whole islets (not encapsulated) stained with calcein AM (green) and ethidium homodimer 1 (red), scale bar of 200µm. (B) Quantification of viable cells per islet, and (C) cellular ATP activity. (D,E) Islets were encapsulated in nanoparticle loaded alginate hydrogels and exposed to low (2mM), then high (20mM) glucose. (D) Insulin secretion 24 hours post encapsulation was measured and (E) the resulting stimulation index was analysed to determine the fold change in insulin secretion on exposure to low and high glucose concentrations. Statistical analysis performed using one way ANOVA with multiple comparisons, statistics in (B,C) represent comparison to untreated islets using paired t tests (GSIS) (D,E) represent comparisons between low and high insulin, compared to islets encapsulated in alginate alone. All graphs show mean values +/- SEM with $p<0.05$*, $p<0.01$**, $p<0.001$***, $p<0.0001$**** and represent mean values from 3-5 independent experiments.

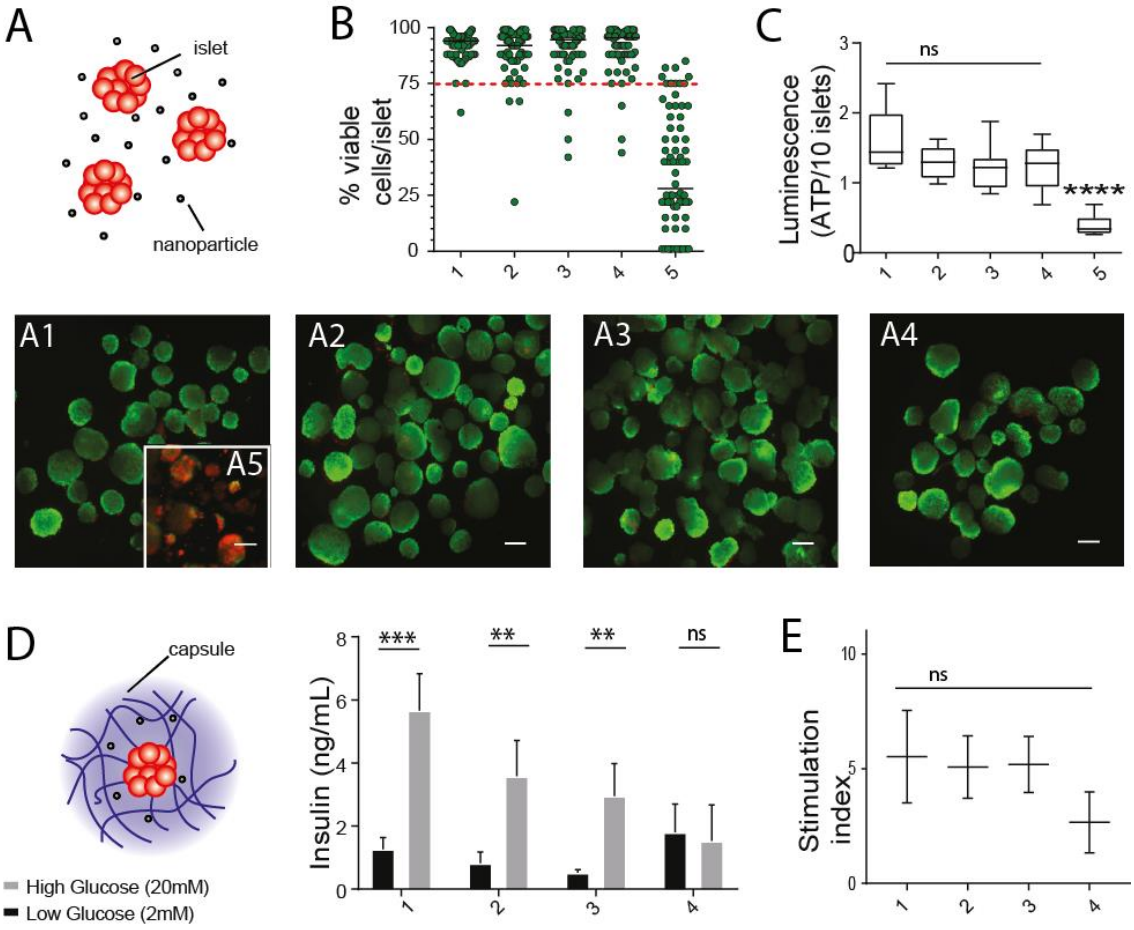

MRI imaging of iron oxide nanoparticle loaded alginate capsules

The inclusion of iron oxide nanoparticles within the alginate capsule renders the capsules responsive to magnetic fields. We therefore evaluated whether hydrogel capsules containing iron oxide nanoparticles could also be visualized post-implantation using MRI, allowing for localization of transplanted capsules (Figure 3A, schematic). First, we fabricated 0.5mm alginate capsules containing iron oxide nanoparticles with nanoparticle concentrations between 0.05-1.00mg/ml (Figure 3B) and embedded these capsules in agarose gels, to stabilize capsule location, before MRI imaging. Capsules were visible *via* MRI at all concentrations tested.

Next, we tested if capsules loaded with 1.00mg/ml iron oxide in two capsule diameters (0.5mm and 1.5mm) were visible once implanted into the IP space of mice. Figure 3B illustrates example MRI images, with several 0.5mm and 1.5mm capsules highlighted using insets; capsules of both sizes were visible using MRI as hypointense regions. We also compared visibility of large capsules containing iron oxide at lower concentrations of 0.25mg/ml, 0.50mg/ml, and 1.00mg/ml (Figure 3C). Results show that in contrast to capsules embedded in agarose gel systems, capsules implanted *in vivo* in the IP space are not easily identifiable at lower iron oxide concentrations of 0.25mg/ml. In contrast, 1.5mm capsules containing iron oxide nanoparticles at concentrations above 0.50mg/ml can be located *in vivo* using this method. The stronger magnetic susceptibility artefacts present at higher iron oxide concentrations make the capsules appear larger in size, thus further facilitating their identification.[25] The identification of these capsules using MRI requires radiographic expertise, and we expect iron oxide concentrations may need to be carefully selected to optimize imaging with other MRI machines with different magnet strengths.

Figure 3: MRI aided localization of nanoparticle loaded capsules (A) Schematic of *in vitro* and *in vivo* imaging of nanoparticle loaded capsules. (B) MRI images of iron oxide nanoparticles encapsulated in 1.5mm alginate hydrogel capsules, and embedded in agarose. (C,D) MRI images of 0.5mm and 1.5mm alginate capsules containing iron oxide nanoparticles implanted into the IP space of C57BL6 mice. Inset panels show zoomed in regions (yellow squares). Inset images are shown twice- with and without asterisks used to mark visible capsules to aid visualization. (C) MRI images of 0.5mm and 1.5mm iron oxide nanoparticle loaded capsules. (D) MRI images of 1.5mm capsules containing concentrations between 0.25-1mg/ml iron oxide implanted into C57BL6 mice. Scale bar 5mm for all images.

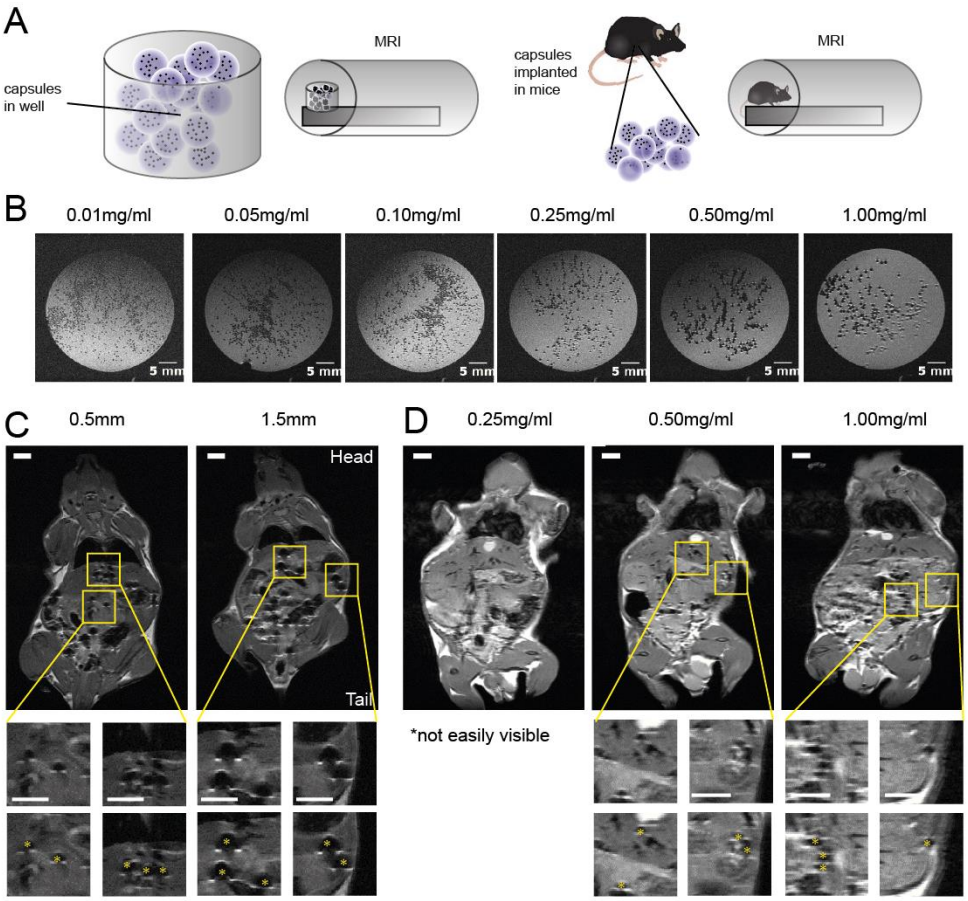

A diabetic mouse model of encapsulated islet transplantation

Our previous results indicated alginate capsules loaded with iron oxide nanoparticles at 1mg/ml could be retrieved on a magnet placed 1-2cm away (Figure 1F), located *in vivo* using MRI (Figure 3C) and were generally well tolerated by islets *in vitro* (Figure 2B-D). To evaluate the clinical utility of this system, we encapsulated rat islets in these nanoparticle alginate systems followed by transplantation into an immune competent diabetic transplant model (Figure 4A, schematic). We then monitored graft function and animal glycemic control, before determining graft location using MRI and subsequent *in vivo* retrieval of encapsulated rat islets (Figure 4B-G).

Localisation and retrieval of encapsulated cell transplants

500 rat islets were encapsulated in nanoparticle loaded alginate hydrogel capsules containing 1mg/ml of NP-PEG or NP-COOH (Figure 4B). These capsules were spherical and nanoparticles appeared well distributed inside (SI Figure 5). We transplanted these capsules into the IP space in STZ induced diabetic mice and show these can be easily identified *via* MRI (Figure 4B). As expected, capsules containing no nanoparticles, and therefore no contrast agent, have limited visibility using MRI. However capsules containing islets with both the NP-PEG and NP-COOH systems can be visualized as hypointense regions using MRI, allowing us to monitor the anatomical distribution of capsules following transplant. Although individual capsules can be located within the abdominal cavity, their distinction from other hypointense structures, and indeed clusters of capsules in the peritoneal cavity, is nevertheless challenging and requires radiographic expertise.

Once capsules had been localized to within the intraperitoneal cavity, we sought to retrieve them through a magnetically assisted surgery. Briefly, we developed a new device for magnetically assisted capsule retrieval *in vivo*, consisting of a peristaltic flushing system

surrounded by an annular magnet to produce a combined mechanical and magnetic retrieval system (Figure 4C). We surgically implanted 200 nanoparticle loaded alginate capsules (NP) into the intraperitoneal space of mice, closed this incision, and in a second surgery (performed within 24 hours of initial implantation) used our device to flush and retrieve capsules, which were then counted. Application of the device for as little as 90 seconds facilitated retrieval of 94% (+/- 3.1% SD) of the iron oxide loaded magnetic capsules (Figure 4C).

In a separate experiment, we transplanted capsules containing islets in alginate capsules loaded with unfunctionalized NP, NP-COOH or NP-PEG into diabetic animals (Figure 4D-G) and successfully surgically retrieved these capsules (Figure 4D,E) following application of a magnetic field for up to 90 seconds. The inclusion of magnetic nanoparticles and the use of our device aids magnetic surgical retrieval; capsules containing magnetic nanoparticles (NP or NP-COOH functionalized) were retrieved at significantly higher yields compared to plain alginate capsules (Figure 4D). Capsules remain intact post-retrieval (SI Figure 5). To evaluate whether these systems could be magnetically retrieved following longer term implantation, we also compared the retrieval of capsules at the 6-8 week timepoint and at 4 months (Figure 4E). We find that capsules can be recovered from the abdominal cavity at later timepoints, and that the capsule volume recovered is not significantly different between 6-8 weeks and 4 months using application of a magnetic field for 90 seconds.

In general, capsules containing iron oxide nanoparticles could be retrieved in greater yields than capsules empty capsules containing no iron oxide nanoparticles (increase in retrieval yield over plain alginate NP: 18.7%, NP-COOH: 44.2%, NP-PEG: 50.6% across all conditions, all timepoints). Surgical retrieval of implanted microcapsules may be influenced by the microcapsule material and any foreign body responses, the location and duration of implantation, and the surgical approach and expertise of the surgeon performing the retrieval.

With further optimization and surgical training, it may be possible to retrieve an even greater proportion of transplanted capsules in this short time frame, reducing the time required for surgical retrieval of encapsulated cell systems.

Figure 4: Application of magnetically retrievable encapsulation systems in a diabetic mouse model (A) Schematic of iron oxide loaded capsules for islet encapsulation and the diabetic mouse model used (B) MRI images of islets co-encapsulated in 1.5mm alginate capsules loaded with iron oxide nanoparticle (either PEGylated (NP-PEG) or carboxylated (NP-COOH)) implanted into C57BL6 mice. Capsules are indicated with red lines- only nanoparticle loaded capsules were visible. (C) Schematic of devices used to test magnetic properties of capsules and retrieval results; 200 NP-capsules were implanted into the IP space of C57B6 mice. In a separate surgery performed within 24 hours, our magnetic device was applied for up to 90 seconds and retrieval assessed (3-4 experiments). Graph represents the proportion of iron oxide loaded capsules that could be collected within 90 seconds. (D) Average volume of capsules retrieved after 6-8 weeks in unfunctionalised, NP, NP-COOH and NP-PEG systems using magnetic retrieval (E) Aggregated data comparing average retrieval volume of magnetic systems (NP, NP-PEG and NP-COOH) after implantation for 6-8 weeks, or 4 months, with application of the magnetic retrieval device limited to 90 seconds. (D,E) All graphs show mean values +/- SEM with p<0.05*, p<0.01**, p<0.001***, p<0.0001**** and represent mean values from 4-10 mice per group. Statistics show a one-way ANOVA with multiple comparisons between individual conditions, compared to unmodified alginate capsules. (F,G) 500 rat islets were encapsulated in alginate, alginate NP, alginate NP-COOH or alginate NP-PEG systems and transplanted into the IP space of STZ-induced diabetic C57B6 mice. (F) Percentage cure rate in various encapsulation systems. A curative euglycemia threshold of 200mg/dL was applied,[12] with failure defined as three consecutive blood glucose measurements above 250mg/ml.[33, 34] (G) Average blood glucose levels of following transplantation of rat islets encapsulated in alginate, or alginate containing nanoparticles. (F,G) Experiments were grouped and conducted 2-3 times and graphs represent average of between 8-12 animals. Statistical analysis was performed using a Mantel-Cox survival curve analysis.

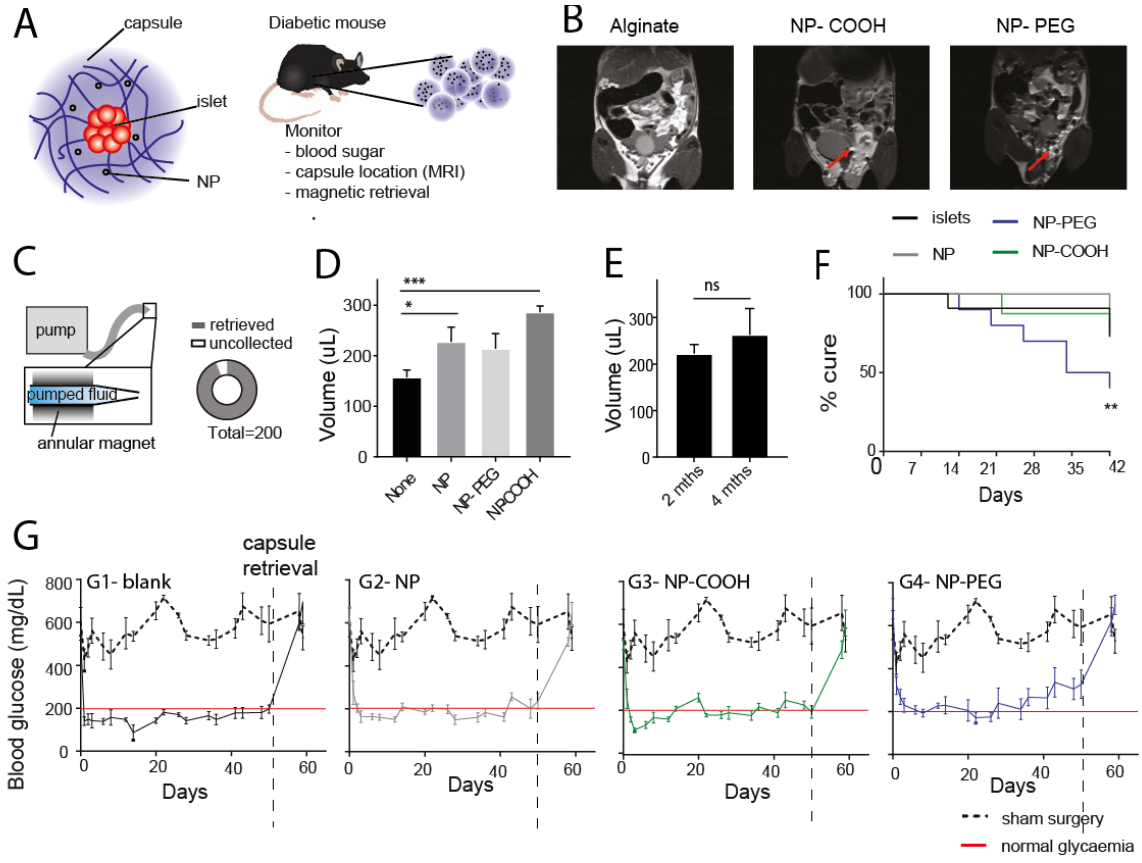

Clinical utility of retrievable microcapsules in islet transplantation in a diabetic mouse model

We evaluated the effect of nanoparticle loaded alginate capsules on a curative dose of rat islets (500/mouse) used to treat C57-B6 diabetic mice. Blood glucose levels were evaluated for 6-8 weeks to determine if these transplants could restore insulin secretion and normoglycemia *in vivo* in mice (Figure 4F, G). Figure 4G represents the relative maintenance of normal glycemia below 200mg/dL following transplant surgery in animals who received a transplant of 500 encapsulated rat islets in alginate or nanoparticle alginate capsules (cure rate). Three consecutive measurements above 250mg/dL post-transplant surgery was considered "transplant failure"[33, 34]; the cure rate therefore describes how long animals retained normal glycemia (remained cured) until transplant failure.

For NP- and NP-COOH systems, islets encapsulated in nanoparticle loaded alginate hydrogels were able to restore normal glycaemia in immunocompetent, diabetic mice without immunosuppression for up to 6-8 weeks, with over 80% of mice remaining normoglycemic at day 42. However, the islets co-encapsulated with NP-PEG functionalized nanoparticles demonstrated significantly impaired function compared to the other systems. NP-PEG systems were able to reduce blood glucose levels to approximately 200mg/dL for the first 4-5 weeks, before blood glucose levels begin to rise. After 6 weeks, the capsules were retrieved as described earlier and blood glucose levels monitored for an additional 3-5 days before termination of the experiment. Blood glucose levels increased immediately after removal of the capsules containing islets, confirming that the encapsulated islets were maintaining normoglycemia in the diabetic mice.

.

Conclusions

For a subset of type I diabetic patients, islet microencapsulation has the potential to enable transplantation of cells and organoids to extra-hepatic transplantation sites, and reduce the need for systemic immune suppression. However, monitoring and retrieving grafts from these sites may prove challenging. Here, we develop a dual-function nanoparticle loaded hydrogel capsule which facilitates magnetically assisted surgical retrieval at the end of transplant lifetimes and enables graft localization *via* MRI.

We have explored capsules loaded with iron oxide nanoparticles functionalized with various ligands (NP-unfunctionalized, NP-COOH or NP-PEG) and compared the properties of these three systems, focusing on islet functionality, capsule tracking *via* MRI, and retrievability. The inclusion of iron oxide nanoparticles within alginate capsules enables magnetic retrieval of capsules *in vitro* and *in vivo*, with the NP-COOH system the most easily retrieved *in vitro*. When coupled with application of a magnetic field for 90 seconds using a magnetically assisted retrieval device, nanoparticle loaded hydrogels facilitate rapid retrieval of up to 94% (+/- 3.1%) of the transplant volume 24 hours post-implantation.

Following transplantation, the inclusion of the iron oxide nanoparticles in the capsule structure at concentrations above 1mg/ml facilitated tracking of encapsulated islets *in vivo* as identifiable, distinct hypointense structures in the IP space using MRI imaging. Islets encapsulated within nanoparticle loaded alginate hydrogels using NP and NP-COOH systems were also able to restore normal glycaemia in immunocompetent, diabetic mice without immunosuppression for up to 6-8 weeks *in vivo*. These capsules remained stable for up to 6 months *in vitro*, with no detectable nanoparticle leaching. In contrast, although PEG functionalized nanoparticle loaded gels were also retrievable, nanoparticle leaching was observed from these hydrogels after a 6 month timeframe, and islet function was impaired *in vitro* and *in vivo*, making them unsuitable for translation. We have therefore identified islets

encapsulated in alginate hydrogels loaded with 1mg/mL of carboxylated iron oxide nanoparticles (NP-COOH) as an optimal system for magnetic retrieval of microencapsulated islets.

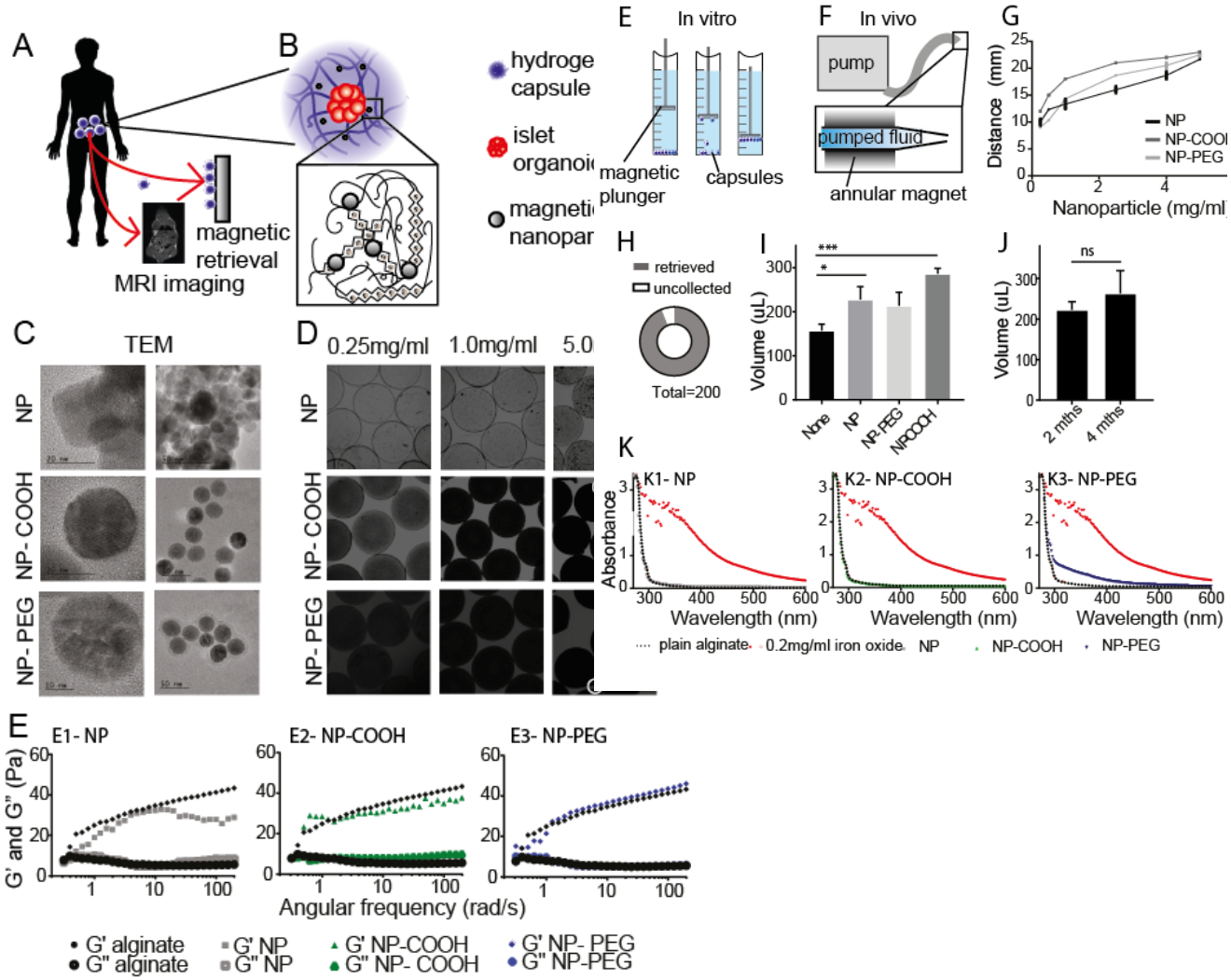

Materials and methods

Reagents were sourced from the following suppliers; $MgCl_2$, $MgSO_4$, and KCl (Mallinckrodt Baker (Paris, KY, USA)), NaCl, mannitol, $CaCl_2$, K_2HPO_4, bovine serum albumin (Sigma-Aldrich (St. Louis, MO, USA)), HEPES buffer, RPMI, FBS, and pen/strep (Gibco (Grand Island, NY)), alginate (SLG20, VLVG and SLG100 (NovaMatrix, Sandvika, Norway), Iron oxide (Fe_3O_4 MTI Corporation, Richmond, CA) or iron nickel oxide nanopowder NP (Fe_2NiO_4, Sigma Aldrich), PEG-NPs (Sigma-Aldrich or OceanTech Nano, (Ocean Nanotech, SMG-20-05)) or COOH-NPs (Sigma-Aldrich or OceanTech Nano). Statistical analysis was performed in GraphPad Prism as described; with **** $p<0.0001$, *** $p<0.001$, ** $p<0.01$, * $p<0.05$.

Nanoparticle characterisation

NP, NP-COOH and NP-PEG nanoparticles were imaged by TEM. Briefly, nanoparticles were loaded onto carbon stubs and imaged in a JEOL 2100 FEG TEM at 120kV. Dynamic light scattering and zeta potential were measured in on a Malvern Zetasizer. Briefly, NP, NP-PEG or NP-COOH were suspended in saline or a 0.1% alginate in saline mixture and loaded into capillary cuvettes before analytical measurements of zeta potential, conductivity and particle size were analysed.

Microcapsule fabrication and testing

Alginate capsules were formed as previously described.[8, 35] In brief, electrostatic droplet generation at 0.1-0.2mL/min under a voltage of 5-10 kV was used to form capsules using a PicoPump syringe pump. Capsules were crosslinked in a 20mM $BaCl_2$ solution and washed in HEPES or in Krebs buffer, and were stored in 0.9% saline containing 2 mM $CaCl_2$ (Ca^{2+}-supplemented saline). To generate iron oxide loaded capsules, iron oxide nanoparticles coated with different functional groups were incorporated into the hydrogel aqueous phase before droplet generation. Nanoparticle leaching was determined by incubating capsules containing NP, NP-PEG or NP-COOH iron oxide nanoparticles in 2mM calcium supplemented saline at

37°C for up to 6 months. Supernatants were taken at regular intervals and absorbance assessed against a nanoparticle standard curve using a TECAN plate reader (300-400nm). Mechanical properties were assessed in bulk hydrogels formed using the nanoparticle loaded aqueous phase for NP, NP-PEG and NP-COOH systems. Briefly, hydrogel disks were crosslinked as described, and parallel plate rheometry was performed at 0.1% strain across the frequency range 0.2 rad/s to 150 rad/s.

Magnetic distance testing

A cylindrical, 1/4″ by 3/4″-diameter rare-earth metal magnet (K&J Magnetics, Plumsteadville, PA) was glued to a syringe plunger with plugged nozzle. Alginate capsules, in ~10-15mL of storage buffer, were layered inside the syringe body. The plunger was submerged in the liquid without disturbing the capsules or trapping air bubbles and gradually lowered until one capsule (for 1.5mm capsules) or two capsules (for 0.5mm capsules) rose toward the magnet. The distance from the bottom of the magnet to the top of the capsules was recorded as the ">0%" magnetic response distance. The plunger was then lowered incrementally until all the capsules had risen to the magnet ("100%" distance).

Islet encapsulation and functional tests

For islet encapsulation, rat islets were isolated as previously described.[35] Briefly, islets were washed in calcium-free Krebs (4.7 mM KCl, 0.58mM $MgSO_4$, 1.2 mM KH_2PO_4, 25 mM HEPES, 135mM NaCl), and encapsulated within 12 hours post-isolation. Capsules containing islets were stored in media in an incubator overnight, and islet function assessed using GSIS (glucose stimulated insulin secretion). Briefly, capsules were washed, and exposed to low KR2 (KR0 + 2mM glucose) for 30 minutes, washed, and then high KR20 (KR0 + 20mM glucose) for 30 minutes. Insulin production was measured by ELISA. Cell viability of islets was assessed post isolation, post encapsulation and post retrieval by dual fluorescence staining with the inclusion/exclusion dyes fluorescein diacetate (FDA) (Sigma) for live cells and propidium iodide (PI) (Sigma) for dead cells. Briefly, naked or encapsulated islets were

rinsed twice with 10ml HBSS (Mediatech) and then mixed with FDA and PI in HBSS. For immunohistological analysis, capsules were fixed in formalin post-retrieval and stained with Newport Green dye (a zinc/insulin dye) and imaged. A fluorescence microscope with bright field view, plus filters for FDA or Newport Green (excitation wavelength 488nm, emission wavelength 520nm) and PI (excitation wavelength 534nm, emission wavelength 617nm) was used to assess the viability of the islets, and to image encapsulated islets and capsules. Percentages of total viable cells within 25–50 whole islets were estimated by a single operator trained in islet isolation protocols.

Microcapsule transplantation and retrieval

Animal procedures were approved by the MIT Committee on Animal Care. STZ-induced diabetic C57BL/6 mice were purchased from Jackson Labs. Surgery was performed under isoflurane anesthesia and post-operative buprenorphine. . Briefly, capsules were infused into the abdominal cavity through an abdominal incision, closed with surgical sutures, tissue glue, and wound clips. Mice were monitored post-surgery, and blood glucose measurements were recorded using a tail prick and AlphaTrak commercial glucose meter (Zoetis, Kalamazoo, MI). A euglycemia threshold of 200mg/dL was applied,[12] with failure defined as three consecutive blood glucose measurements above 250mg/ml.[33, 34] Both survival and euthanized retrieval surgeries were performed. The incision site was opened and IP space was flushed with Krebs solution to enable capsule collection. For non-terminal retrievals, mice were anaesthetized as described above. A surgical flushing instrument aided mechanical and magnetic retrieval of capsules. An annular magnet (i.e. 1/8 in, o.d. ¼ in x ¼ in) was fixed to a pipette hose and peristaltic pump (VWR, Radnor, PA). Sterile saline was used to flush and retrieve capsules. Magnetic capsules loosely attached to the magnet, and could be flushed off into a collection chamber.

MRI imaging

Capsules were embedded into agarose gels prior to *in vitro* imaging, or were transplanted into the IP cavity of mice as described. Mice were anaesthetized and placed in the supine position within a volume coil of a 7T preclinical MRI system (Varian 7T/310/ASR, Agilent). Vital signs and temperature were continuously monitored. Respiratory gating was performed for motion artifact correction. Images were collected using 1mm thick coronal slices of 50mmx50mm field of view. A fast spin echo pulse sequence (TR=2000 ms, TE=12.7 ms, Data matrix: 256 x 256, 2 averages) was used. Data was stored in DICOM format and was visualized using MATLAB.

Acknowledgements

The authors gratefully acknowledge Jenifer Hollister Lock and the Joslin Diabetes Centre, Boston Children's Hospital, for the isolation of islets used in this study. We also thank the Koch Institute Swanson Biotechnology Center for access to core facilities and for technical support, specifically; Wei Huang and the Animal Imaging & Preclinical Testing Core for assistance with MRI imaging, Yun Dong Soo for TEM imaging and Margaret Bisher for SEM imaging and materials preparation from the Nanotechnology Materials Core. This work was supported in part by funding provided by the Juvenile Diabetes Research Foundation, the Helmsley Charitable Trust and the Koch Institute Support Grant P30-CA14051. DD gratefully acknowledges an EPSRC E-TERM Fellowship and a Marie Sklodowska Curie Fellowship.

References

[1] A.M.J. Shapiro, J.R.T. Lakey, E.A. Ryan, G.S. Korbutt, E. Toth, G.L. Warnock, N.M. Kneteman, R.V. Rajotte, Islet transplantation in seven patients with type 1 diabetes mellitus using a glucocorticoid-free immunosuppressive regimen, New England Journal of Medicine 343(4) (2000) 230-238.
[2] A.M.J. Shapiro, C. Ricordi, B.J. Hering, H. Auchincloss, R. Lindblad, P. Robertson, A. Secchi, M.D. Brendel, T. Berney, D.C. Brennan, E. Cagliero, R. Alejandro, E.A. Ryan, B. DiMercurio, P. Morel, K.S. Polonsky, J.A. Reems, R.G. Bretzel, F. Bertuzzi, T. Froud, R. Kandaswamy, D.E.R. Sutherland, G. Eisenbarth, M. Segal, J. Preiksaitis, G.S. Korbutt, F.B. Barton, L. Viviano, V. Seyfert-Margolis, J. Bluestone, J.R.T. Lakey, International trial of the edmonton protocol for islet transplantation, New England Journal of Medicine 355(13) (2006) 1318-1330.
[3] F.B. Barton, M.R. Rickels, R. Alejandro, B.J. Hering, S. Wease, B. Naziruddin, J. Oberholzer, J.S. Odorico, M.R. Garfinkel, M. Levy, F. Pattou, T. Berney, A. Secchi, S. Messinger, P.A. Senior, P. Maffi, A. Posselt, P.G. Stock, D.B. Kaufman, X.R. Luo, F. Kandeel, E. Cagliero, N.A. Turgeon, P. Witkowski, A. Naji, P.J. O'Connell, C. Greenbaum, Y.C. Kudva, K.L. Brayman, M.J. Aull, C. Larsen, T.W.H. Kay, L.A. Fernandez, M.C. Vantyghem, M. Bellin, A.M.J. Shapiro, Improvement in Outcomes of Clinical Islet Transplantation: 1999-2010, Diabetes Care 35(7) (2012) 1436-1445.
[4] E.A. Ryan, J.R.T. Lakey, R.V. Rajotte, G.S. Korbutt, T. Kin, S. Imes, A. Rabinovitch, J.F. Elliott, D. Bigam, N.M. Kneteman, G.L. Wanock, I. Larsen, A.M.J. Shapiro, Clinical outcomes and insulin secretion after islet transplantation with the edmonton protocol, Diabetes 50(4) (2001) 710-719.
[5] D.M. Harlan, N.S. Kenyon, O. Korsgren, B.O. Roep, S. Diabet, Current Advances and Travails in Islet Transplantation, Diabetes 58(10) (2009) 2175-2184.
[6] T.T. Dang, A.V. Thai, J. Cohen, J.E. Slosberg, K. Siniakowicz, J.C. Doloff, M.L. Ma, J. Hollister-Lock, K.M. Tang, Z. Gu, H. Cheng, G.C. Weir, R. Langer, D.G. Anderson, Enhanced function of immuno-isolated islets in diabetes therapy by co-encapsulation with an anti-inflammatory drug, Biomaterials 34(23) (2013) 5792-5801.
[7] M.L. Ma, A. Chiu, G. Sahay, J.C. Doloff, N. Dholakia, R. Thakrar, J. Cohen, A. Vegas, D.L. Chen, K.M. Bratlie, T. Dang, R.L. York, J. Hollister-Lock, G.C. Weir, D.G. Anderson, Core-Shell Hydrogel Microcapsules for Improved Islets Encapsulation, Advanced Healthcare Materials 2(5) (2013) 667-672.
[8] A.J. Vegas, O. Veiseh, J.C. Doloff, M. Ma, H.H. Tam, K. Bratlie, J. Li, A.R. Bader, E. Langan, K. Olejnik, P. Fenton, J.W. Kang, J. Hollister-Locke, M.A. Bochenek, A. Chiu, S. Siebert, K. Tang, S. Jhunjhunwala, S. Aresta-Dasilva, N. Dholakia, R. Thakrar, T. Vietti, M. Chen, J. Cohen, K. Siniakowicz, M. Qi, J. McGarrigle, S. Lyle, D.M. Harlan, D.L. Greiner, J. Oberholzer, G.C. Weir, R. Langer, D.G. Anderson, Combinatorial hydrogel library enables identification of materials that mitigate the foreign body response in primates, Nat Biotechnol 34(3) (2016) 345-+.
[9] O. Veiseh, J.C. Doloff, M. Ma, A.J. Vegas, H.H. Tam, A.R. Bader, J. Li, E. Langan, J. Wyckoff, W.S. Loo, S. Jhunjhunwala, A. Chiu, S. Siebert, K. Tang, J. Hollister-Lock, S. Aresta-Dasilva, M. Bochenek, J. Mendoza-Elias, Y. Wang, M. Qi, D.M. Lavin, M. Chen, N. Dholakia, R. Thakrar, I. Lacik, G.C. Weir, J. Oberholzer, D.L. Greiner, R. Langer, D.G. Anderson, Size- and shape-dependent foreign body immune response to materials implanted in rodents and non-human primates, Nat. Mater. 14(6) (2015) 643-U125.
[10] G. Basta, P. Montanucci, G. Luca, C. Boselli, G. Noya, B. Barbaro, M.R.G. Qi, K.P. Kinzer, J. Oberholzer, R. Calafiore, Long-Term Metabolic and Immunological Follow-Up of Nonimmunosuppressed Patients With Type 1 Diabetes Treated With Microencapsulated Islet Allografts, Diabetes Care 34(11) (2011) 2406-2409.
[11] D. Dufrane, R.M. Goebbels, A. Saliez, Y. Guiot, P. Gianello, Six-month survival of microencapsulated pig islets and alginate biocompatibility in primates: Proof of concept, Transplantation 81(9) (2006) 1345-1353.
[12] A.J. Vegas, O. Veiseh, M. Guertler, J.R. Millman, F.W. Pagliuca, A.R. Bader, J.C. Doloff, J. Li, M. Chen, K. Olejnik, H.H. Tam, S. Jhunjhunwala, E. Langan, S. Aresta-Dasilva, S. Gandham, J.J. McGarrigle, M.A. Bochenek, J. Hollister-Lock, J. Oberholzer, D.L. Greiner, G.C. Weir, D.A. Melton, R. Langer, D.G.

Anderson, Long-term glycemic control using polymer-encapsulated human stem cell-derived beta cells in immune-competent mice, Nat Med 22(3) (2016) 306-311.
[13] M. Omami, J.J. McGarrigle, M. Reedy, D. Isa, S. Ghani, E. Marchese, M.A. Bochenek, M. Longi, Y. Xing, I. Joshi, Y. Wang, J. Oberholzer, Islet Microencapsulation: Strategies and Clinical Status in Diabetes, Curr. Diabetes Rep. 17(7) (2017) 7.
[14] M.A. Bochenek, O. Veiseh, A.J. Vegas, J.J. McGarrigle, M. Qi, E. Marchese, M. Omami, J.C. Doloff, J. Mendoza-Elias, M. Nourmohammadzadeh, A. Khan, C.C. Yeh, Y. Xing, D. Isa, S. Ghani, J. Li, C. Landry, A.R. Bader, K. Olejnik, M. Chen, J. Hollister-Lock, Y. Wang, D.L. Greiner, G.C. Weir, B.L. Strand, A.M.A. Rokstad, I. Lacik, R. Langer, D.G. Anderson, J. Oberholzer, Alginate encapsulation as long-term immune protection of allogeneic pancreatic islet cells transplanted into the omental bursa of macaques, Nature Biomedical Engineering 2(11) (2018) 810-821.
[15] A. Balhuizen, S. Massa, I. Mathijs, J.V. Turatsinze, J. De Vos, S. Demine, C. Xavier, O. Villate, I. Millard, D. Egrise, C. Capito, R. Scharfmann, P. In't Veld, P. Marchetti, S. Muyldermans, S. Goldman, T. Lahoutte, L. Bouwens, D.L. Eizirik, N. Devoogdt, A nanobody-based tracer targeting DPP6 for non-invasive imaging of human pancreatic endocrine cells, Scientific Reports 7 (2017).
[16] O.A. El-Kawy, J.A. Garcia-Horsman, Tc-99m-labeled glimepiride as a tracer for targeting pancreatic beta-cells mass: preparation and preclinical evaluation, Journal of Radioanalytical and Nuclear Chemistry 314(3) (2017) 2539-2550.
[17] O. Eriksson, M. Laughlin, M. Brom, P. Nuutila, M. Roden, A. Hwa, R. Bonadonna, M. Gotthardt, In vivo imaging of beta cells with radiotracers: state of the art, prospects and recommendations for development and use, Diabetologia 59(7) (2016) 1340-1349.
[18] R. Hernandez, S.A. Graves, T. Gregg, H.R. VanDeusen, R.J. Fenske, H.N. Wienkes, C.G. England, H.F. Valdovinos, J.J. Jeffery, T.E. Barnhart, G.W. Severin, R.J. Nickles, M.E. Kimple, M.J. Merrins, W. Cai, Radiomanganese PET Detects Changes in Functional beta-Cell Mass in Mouse Models of Diabetes, Diabetes 66(8) (2017) 2163-2174.
[19] A. Jodal, R. Schibli, M. Behe, Targets and probes for non-invasive imaging of beta-cells, European Journal of Nuclear Medicine and Molecular Imaging 44(4) (2017) 712-727.
[20] H. Kimura, Y. Ogawa, H. Fujimoto, E. Mukai, H. Kawashima, K. Arimitsu, K. Toyoda, N. Fujita, Y. Yagi, K. Hamamatsu, T. Murakami, A. Murakami, M. Ono, Y. Nakamoto, K. Togashi, N. Inagaki, H. Saji, Evaluation of F-18-labeled exendin(9-39) derivatives targeting glucagon-like peptide-1 receptor for pancreatic beta-cell imaging, Bioorganic & Medicinal Chemistry 26(2) (2018) 463-469.
[21] S. Sarkis, F. Silencieux, K.E. Markwick, M.A. Fortin, C.A. Hoesli, Magnetic Resonance Imaging of Alginate Beads Containing Pancreatic Beta Cells and Paramagnetic Nanoparticles, Acs Biomaterials Science & Engineering 3(12) (2017) 3576-3587.
[22] C.T. Yang, K.K. Ghosh, P. Padmanabhan, O. Langer, J. Liu, C. Halldin, B.Z. Gulyas, PET probes for imaging pancreatic islet cells, Clinical and Translational Imaging 5(6) (2017) 507-523.
[23] C. Adams, L.L. Israel, S. Ostrovsky, A. Taylor, H. Poptani, J.P. Lellouche, D. Chari, Development of Multifunctional Magnetic Nanoparticles for Genetic Engineering and Tracking of Neural Stem Cells, Advanced Healthcare Materials 5(7) (2016) 841-849.
[24] Z.Q. Zhang, S.C. Song, Thermosensitive/superparamagnetic iron oxide nanoparticle-loaded nanocapsule hydrogels for multiple cancer hyperthermia, Biomaterials 106 (2016) 13-23.
[25] V. Spanoudaki, J.C. Doloff, W. Huang, S.R. Norcross, S. Farah, R. Langer, D.G. Anderson, Simultaneous spatiotemporal tracking and oxygen sensing of transient implants in vivo using hot-spot MRI and machine learning, Proceedings of the National Academy of Sciences of the United States of America 116(11) (2019) 4861-4870.
[26] M.S. Shoichet, R.H. Li, M.L. White, S.R. Winn, Stability of hydrogels used in cell encapsulation: An in vitro comparison of alginate and agarose, Biotechnol. Bioeng. 50(4) (1996) 374-381.
[27] E.A. Appel, M.W. Tibbitt, J.M. Greer, O.S. Fenton, K. Kreuels, D.G. Anderson, R. Langer, Exploiting Electrostatic Interactions in Polymer-Nanoparticle Hydrogels, ACS Macro Lett. 4(8) (2015) 848-852.
[28] J. Huwyler, D.F. Wu, W.M. Pardridge, Brain drug delivery of small molecules using immunoliposomes, Proceedings of the National Academy of Sciences of the United States of America 93(24) (1996) 14164-14169.

[29] B. Naeye, K. Raemdonck, K. Remaut, B. Sproat, J. Demeester, S.C. De Smedt, PEGylation of biodegradable dextran nanogels for siRNA delivery, European Journal of Pharmaceutical Sciences 40(4) (2010) 342-351.
[30] M. Ogris, S. Brunner, S. Schuller, R. Kircheis, E. Wagner, PEGylated DNA/transferrin-PEI complexes: reduced interaction with blood components, extended circulation in blood and potential for systemic gene delivery, Gene Therapy 6(4) (1999) 595-605.
[31] T. Simon-Yarza, F.R. Formiga, E. Tamayo, B. Pelacho, F. Prosper, M.J. Blanco-Prieto, PEGylated-PLGA microparticles containing VEGF for long term drug delivery, International Journal of Pharmaceutics 440(1) (2013) 13-18.
[32] V. Uskokovic, P.P. Lee, L.A. Walsh, K.E. Fischer, T.A. Desai, PEGylated silicon nanowire coated silica microparticles for drug delivery across intestinal epithelium, Biomaterials 33(5) (2012) 1663-1672.
[33] E. Cantarelli, A. Citro, S. Marzorati, R. Melzi, M. Scavini, L. Piemonti, Murine animal models for preclinical islet transplantation No model fits all (research purposes), Islets 5(2) (2013) 79-86.
[34] S. Pellegrini, E. Cantarelli, V. Sordi, R. Nano, L. Piemonti, The state of the art of islet transplantation and cell therapy in type 1 diabetes, Acta Diabetologica 53(5) (2016) 683-691.
[35] O. Veiseh, J.C. Doloff, M. Ma, A.J. Vegas, H.H. Tam, A.R. Bader, J. Li, E. Langan, J. Wyckoff, W.S. Loo, S. Jhunjhunwala, A. Chiu, S. Siebert, K. Tang, J. Hollister-Lock, S. Aresta-Dasilva, M. Bochenek, J. Mendoza-Elias, Y. Wang, M. Qi, D.M. Lavin, M. Chen, N. Dholakia, R. Thakrar, I. Lacík, G.C. Weir, J. Oberholzer, D.L. Greiner, R. Langer, D.G. Anderson, Size- and shape-dependent foreign body immune response to materials implanted in rodents and non-human primates, Nature materials 14(6) (2015) 643-651.